The transition from single phonon to multiphonon energy transfer in atom–surface collisions

F. Hofmann and J. P. Toennies
Max Planck Institut für Strömungsforschung, Bunsenstrasse 10, 37073 Göttingen, Germany

J. R. Manson
Department of Physics and Astronomy, Clemson University, Clemson, South Carolina 29634

(Received 26 August 1996; accepted 4 October 1996)

The angular distributions and time-of-flight spectra of nearly monoenergetic He atoms with incident energies of 82 meV and 112 meV have been measured after scattering from a clean Cu(001) surface over a large range of crystal temperatures from 100 K to 1000 K. With increasing temperatures the sharp diffraction and phonon peaks of the low temperature quantum regime become broad and featureless as expected for the multiphonon classical regime. The results are compared with a quantum mechanical theory which is able to explain the height, position, width, and area under the multiphonon maximum. In the classical regime, the temperature dependence of the inelastic intensity indicates that the He atoms are reflected by a smooth vibrating barrier presumably due to the surface electron density, and not by a lattice of discrete repulsive surface atomic cores. © *1997 American Institute of Physics.* [S0021-9606(97)02102-8]

I. INTRODUCTION

Energy transfer in gas–surface interactions has been discussed in mathematically quantitative terms since Knudsen's analysis of the accommodation coefficient.[1] Modern high resolution helium atom surface scattering (HAS) experiments provide a great deal of information on the energy transfer process particularly in the quantum mechanical regime of low energies and low surface temperatures.[2] Measurements of diffraction and single quantum inelastic exchanges have provided important new information on surface structure, surface vibrations (including complete surface phonon dispersion relations) and atom–surface interaction potentials.[3–5]

These results cannot easily be employed for understanding the elementary processes of energy accommodation, trapping, and sticking of the more common heavier rare gases and molecules such as O_2, N_2, and CO. These processes are not only of interest for many technological applications such as hypersonic flows but are of direct relevance for the understanding of chemical reactions on surfaces. Because of the greater particle masses these interactions are dominated by the more complicated multiphonon surface collision dynamics and to an unknown extent by electron–hole pair creation. Even larger energy transfers are involved in dissociative chemisorption in which energies of the order of several electron volts have to be dissipated locally.

In recent years considerable experimental and theoretical effort has gone into understanding the surface interactions of heavy molecules. In one set of experiments related to understanding chemisorption the sticking of a beam of molecules is studied as a function of the angle of incidence, kinetic energy, and more recently also as a function of internal energy.[6,7] The interpretation of these experiments is complicated since a number of different elementary processes are involved and the theory requires a knowledge of a multidimensional hypersurface of which important parts are only recently becoming available for simple metal systems such as H_2/Cu(001) and H_2/Pd(001).[8–14] In another set of molecular beam experiments the scattered atoms and molecules are analyzed for their final angular and velocity distributions.[15–19] Instead of sharp features as in the case of the HAS experiments the time-of-flight spectra usually exhibit two broad peaks, a relatively fast peak corresponding to inelastic scattering, and a slow peak due to particles which were temporarily trapped on the surface and partially accommodated. The angular distributions are usually broad and frequently bimodal in accord with the two processes described above. Because of the broadness of the features the interpretation is not at all straightforward. This is illustrated by the fact that in some instances simple statistical models can also explain the data.[20] Nevertheless, substantial progress has been made. For example Rettner and colleagues have succeeded in extracting a potential for the Xe/Pt(111) system from an interpretation of such scattering experiments.[21]

In the present paper we have adopted a different approach in an attempt to develop and test a theory for dealing with multiphonon interactions in a controlled way. In a previous study we carried out an extensive examination of the one-phonon interactions of He atoms with the Cu(001) surface in the quantum regime.[22] Here the same system is studied as the surface temperature is increased so that the interaction evolves gradually from the quantum single phonon regime to the classical multiphonon regime.

In the low energy quantum regime the major features in the energy resolved distribution are the purely elastic peaks and single phonon peaks. The elastic features arise from diffraction or from scattering by defects and impurities on the surface, while sharp single phonon peaks result from coherent interactions with localized surface modes. These sharp quantum features rise out of a broad continuous inelastic background. This background can be due to several sources, the most important ones being multiphonon scattering, single

 0021-9606/97/106(3)/1234/14/$10.00

quantum interactions with bulk phonon modes, and inelastic scattering from defects, disordered regions, and impurities. At very low energies and surface temperatures the single phonon events are predominant, but with increasing beam energies and surface temperatures the single quantum peaks decrease in intensity while the broad diffuse multiphonon background increases in intensity and width.[23] The quantum peaks decrease in intensity according to the well known Debye–Waller behavior and the point at which they disappear altogether marks the onset of the classical regime. At the highest surface temperatures studied here the limit of large phonon quantum numbers is reached and the system becomes fully classical as expected from the correspondence principle of quantum mechanics.[24]

In the classical regime there are no longer any distinct elastic scattering peaks, and the broad distribution of final energies has a maximum at an energy which depends on the final angle. With further increasing surface temperature or with increasing incident energy, the distribution of intensities spreads over a larger range of energy transfer as more final scattering channels become available. Unitarity implies that at angles where the multiphonon intensity is initially large the maximum peak intensity decreases with increasing surface temperature and energy in order that the total number of scattered particles remains constant. However, at larger angles away from the peak at low temperatures the maximum may actually increase at first, because multiphonon intensity is reaching those channels for the first time. Only later at even higher temperatures and incident energies does the intensity in these regions begin to decrease.

To analyze the data we use a multiphonon theory developed earlier.[25,26] Since the important physical properties such as the He-surface potential and the surface phonon dispersion curves have been well characterized in the earlier one-phonon experiments[22] it is possible to extract information on the change in the fundamental interaction in the high energy regime. The measured intensities are found to agree well with a quantum mechanical scattering theory which has been extended into the classical multiquantum regime. In the classical regime the scattered intensity as a function of incident and final momenta can be formulated in a closed form expression resembling a skewed Gaussian function[25,27,28] whose maximum intensity is dictated by a multiplicative envelope function.

The theory predicts distinct differences in the classical scattering depending upon whether the crystal is regarded as a collection of discrete scattering centers or as a smooth continuum surface.[25] There is now ample evidence[29,30] that in the one-phonon regime the potentials for the He atoms interacting with metal surfaces are smooth and nearly free of any corrugation at the classical turning point as shown in Fig. 1. This is attributed to the Pauli exchange repulsion between the electrons of the He atom and the tail of the metallic free electron gas which extends far from the surface.[31] At some point this approximation breaks down as the incident energy becomes larger, as suggested by several He atom diffraction studies which reveal an increase in corrugation with increasing energy.[32,33] Thus in the extreme high energy limit the corrugation should approach that of the classical turning points surrounding discrete ionic cores. For the temperature dependence of the multiphonon envelope function, the discrete model predicts maximum intensities varying as $T_S^{-1/2}$ whereas the flat surface continuum model predicts a $T_S^{-3/2}$ dependence. The present measurements of the multiphonon temperature dependence demonstrate convincingly that in the classical regime the He atoms scatter from a continuum surface with no indication of scattering from a discrete lattice of individual surface atom cores.[34] It is interesting to note that models similar to the discrete model have been frequently used in the past for even low temperature quantum scattering calculations.[35–38]

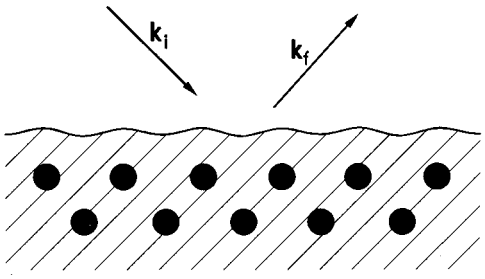

FIG. 1. Illustration of a surface with a smooth continuously distributed classical turning point with the ionic cores shown. The present calculations use this model as opposed to a model in which the surface is described by discrete scattering centers.

The remainder of this paper is organized in the following way. In Sec. II we briefly discuss the experimental apparatus. In Sec. III we outline the theory which is used to analyze the experiment. The observed scattering intensities as functions of scattering angles, energy exchange, and surface temperature, are presented in Sec. IV together with comparisons with theory. A few conclusions and a discussion of the implications of the agreement between theory and experiment are given in Sec. V.

II. EXPERIMENT

The essential features of the experimental apparatus have been described elsewhere[2,39] so we present only a brief description here. The He atom incident beam is produced by an adiabatic expansion through a thin-walled 10 μm diam orifice from a high pressure ($\approx$400 bar). The beam then passes 10–20 mm downstream through a long (25 mm) conical skimmer with a 0.7 mm diam opening. The beam is subsequently chopped into short pulses before scattering off the crystal target and then travels a time-of-flight (TOF) path of approximately 1.4 m before arriving at the electron bombardment ionization magnetic mass spectrometer. The detector is located in the common plane of the incident beam and the normal to the surface and is positioned at a fixed angle of 95.8° with respect to the incident beam. Different scattering angles are accessed by rotating the target around an axis normal to the scattering plane.

When operating in the time-of-flight (TOF) mode with a chopped beam, the overall sensitivity ranges from approximately 5 counts/s (background) to a maximum of more than

10^7 counts/s depending on the beam energy and target temperature. The overall energy resolution, at the relatively large beam energies of $E_i \approx 100$ meV used here, is mainly determined by the inherent velocity spread $\Delta v/v \lesssim 3.5\%$ of the He beam, leading to an energy resolution of $\Delta E \approx 7.5$ meV for $E_i = 113$ meV and $\Delta E \approx 4$ meV for $E_i = 82$ meV. The angular resolution is determined by the detector acceptance angle which is about 0.2° both in- and out-of-plane.

The Cu(001) single crystal was oriented to better than 0.2° with respect to the (001) face, mechanically polished and further prepared *in situ* by repeated cycles of sputtering with 800 eV Ar^+ ions at a temperature of 500 K followed by annealing at 850 K for 10 min. The cleaning procedure was repeated until no contamination within the 0.5% sensitivity of the Auger cylinder mirror analyzer could be detected. After prolonged measurement times exceeding 2 h at elevated temperatures small traces of sulfur contamination in the percent of a monolayer range were found. The above cleaning procedure was therefore repeated every 2 h. The crystal is mounted on a manipulator with an angular accuracy of $\leqslant 0.1°$. Crystal temperatures ranging from 35 K up to 1200 K could be accessed. These temperatures were measured with a Chromel/Alumel thermocouple clamped onto the crystal surface and could be controlled with a relative stability of ± 0.5 K and an absolute accuracy of $\approx \pm 5$ K.

III. REVIEW OF THE THEORY

The formal theory of atom scattering from a crystal surface lattice starts from the very general Hamiltonian $H = H_p + H_c + V$, where H_p is the free projectile Hamiltonian, H_c is the Hamiltonian of the isolated crystal, and V is the interaction potential coupling the two systems.[25,27,40] This complex problem can be reduced to a tractable form appropriate to the problem at hand by application of the semiclassical approximation with classically allowed trajectories and the quick collision approximation.[40] Within these approximations the result for the differential reflection coefficient, which gives the fraction of particles scattered into final energy interval dE_f and final solid angle $d\Omega_f$, is[26,41]

$$\frac{dR}{d\Omega_f dE_f} = \frac{m^2 |\mathbf{k}_f| L^4}{(2\pi)^3 \hbar^5 k_{iz}} |\tau_{fi}|^2 e^{-2W(\mathbf{k})} \times \int_{-\infty}^{+\infty} dt e^{-i\Delta E t/\hbar} \sum_l e^{i\mathbf{K}\cdot\mathbf{R}_l} e^{\langle\langle \mathbf{k}\cdot\mathbf{u}_0(0)\mathbf{k}\cdot\mathbf{u}_l(t)\rangle\rangle}, \tag{1}$$

where $\Delta E = E_f - E_i$ is the energy exchanged between the particle and surface, $\mathbf{k} = \mathbf{k}_f - \mathbf{k}_i$ is the scattering vector, m is the projectile mass, L is a quantization length, and $\mathbf{u}_l(t)$ is the displacement vector of the lth surface unit cell located at position vector $\mathbf{R}_l$. Moreover the particle wave vectors $\mathbf{k}_q$ are expressed in terms of components $\mathbf{K}_q$ parallel to the surface and k_{qz} perpendicular to the surface. The Debye–Waller factor $\exp[-2W(\mathbf{k})]$ appearing in Eq. (1) takes on the usual form in terms of the equal-time displacement correlation function according to $2W(\mathbf{k}) = \langle\langle [\mathbf{k}\cdot\mathbf{u}_l(t)]^2 \rangle\rangle$.[42] Approximating the phonon distribution of the solid by a Debye frequency distribution, as we will do here, provides a very useful and commonly used expression for the Debye–Waller exponent

$$2W(\mathbf{k}) = \frac{3\hbar^2 \mathbf{k}^2 T_S}{M k_B \Theta_D^2}, \tag{2}$$

where M is the crystal atom mass, Θ_D is the Debye temperature, and k_B is Boltzmann's constant. $2W(\mathbf{k})$ can be interpreted as the average number of phonons excited in a collision.

Within this approximation the scattering amplitude τ_{fi} is determined to be the off-energy-shell transition matrix for scattering of the projectile by a unit cell of the purely elastic part of the interaction potential V. Within the approximations made Eq. (1) provides a complete description of the scattering process in that it contains the elastic contribution as well as all numbers of phonon exchange. In spite of its approximate form, the simple expression for the single phonon intensity produced by this theory describes quite well the energy, temperature, and parallel momentum dependence of the single phonon intensities measured for He scattering from Cu(001).[22] The expansion of the exponential of the displacement correlation function produces an ordered series in terms of numbers of exchanged phonons. In order to obtain the multiphonon part, the elastic and single phonon contributions are subtracted from Eq. (1). This multiphonon theory has previously been able to explain the shape and temperature dependence of the background in a number of atom–surface scattering systems.[43–45]

In the classical limit of high temperatures and large projectile energies Eq. (1) can be evaluated in closed form to give[25,26]

$$\frac{dR}{d\Omega_f dE_f} = \frac{m^2 |\mathbf{k}_f| L^4}{8\pi^3 \hbar^4 k_{iz}} |\tau_{fi}|^2 \left(\frac{\pi}{\Delta E_0 k_B T_S} \right)^{1/2} \times \exp\left[-\frac{(\Delta E + \Delta E_0)^2}{4 k_B T_S \Delta E_0} \right]. \tag{3}$$

where the most probable energy shift is given by the recoil energy of an individual surface atom $\Delta E_0 = \hbar^2 \mathbf{k}^2 / 2M$. This simple recoil expression arises in the classical limit where the quantum mechanical scattering correlation length becomes small and the collisions between the projectile and the surface reduce to pairwise collisions with the surface atoms. The classical limit is identical for any surface phonon model which produces a reasonably physical distribution of vibrational modes. The condition for the validity of Eq. (3) is that $2W(\mathbf{k})$ is large, and in practice one finds approximately $2W(\mathbf{k}) > 6$,[34,47] so that on average at least six phonons must be transferred in the collision. Interestingly, the Debye–Waller factor does not appear explicitly in Eq. (3). The Debye–Waller factor is canceled by a factor arising from the exponentiated correlation function in Eq. (1) leaving behind the Gaussian-type function of Eq. (3).

For the case of a smooth potential, see Fig. 1, the theory leading to Eq. (1) can be modified by regarding the surface

as being continuous rather than a set of scattering centers located within the unit cells. The result, appropriate for a flat continuous surface is

$$\frac{dR}{d\Omega_f dE_f} = \frac{m^2|\mathbf{k}_f|L^4}{(2\pi)^3\hbar^5 k_{iz} S_{\text{u.c.}}} |\tau_{fi}|^2 e^{-2W(\mathbf{k})} \times \int_{-\infty}^{+\infty} dt e^{-i\Delta E t/\hbar} \int d\mathbf{R} e^{i\mathbf{K}\cdot\mathbf{R}} e^{\langle\langle(\mathbf{k}\cdot\mathbf{u}(0,0)\mathbf{k}\cdot\mathbf{u}(\mathbf{R},t)\rangle\rangle}, \tag{4}$$

where $S_{\text{u.c.}}$ is the area of a surface unit cell.[40]

Equation (4) can be readily evaluated in the classical limit, and the result is somewhat different from Eq. (3),[27,40]

$$\frac{dR}{d\Omega_f dE_f} = \frac{m^2|\mathbf{k}_f|L^4\omega_R^2}{(2\pi)^4\hbar^2 k_{iz}} |\tau_{fi}|^2 \left(\frac{\pi}{\Delta E_0 k_B T_S}\right)^{3/2} \times \exp\left[-\frac{(\Delta E+\Delta E_0)^2 + 2\hbar^2 v_R^2 K^2}{4k_B T_S \Delta E_0}\right], \tag{5}$$

where v_R is a weighted average of surface phonon velocities parallel to the surface and ω_R, given by $\omega_R^2 = 4\pi v_R^2/S_{\text{u.c.}}$, is the corresponding characteristic frequency.[27] The essential differences with the discrete limit of Eq. (3) is that Eq. (5) has a pre-exponential envelope function varying as $(\Delta E_0 T_S)^{-3/2}$ rather than $(\Delta E_0 T_S)^{-1/2}$, and there is an additional Gaussian-type term in the parallel momentum transfer **K** arising from correlated vibrations parallel to the surface. In this case the classical expression does depend on the model used for the phonon modes, but only through the characteristic velocity v_R. Equation (5) is essentially the expression first obtained by Brako and Newns,[27] but here the energy shift ΔE_0 is completely specified and the scattering form factor $|\tau_{fi}|^2$ arises naturally out of the theory.

For the calculations presented below we have chosen the transition matrix amplitude τ_{fi} to be the product of the Gaussian cutoff function for parallel momentum with range Q_c (Ref. 48) and the Mott–Jackson matrix element $v_{\text{M–J}}$ in perpendicular momentum for a repulsive potential of the form $\exp[-\beta z]$,[49,50] where z is the coordinate normal to the surface,

$$\tau_{fi} = e^{-K^2/2Q_c^2} v_{\text{M–J}}. \tag{6}$$

This simple expression for the scattering amplitude is derived from the distorted wave Born approximation and has been utilized for describing the inelastic scattering, both single phonon and multiphonon, for several systems.[22,51]

For all calculations presented here the displacement correlation functions necessary for Eq. (4) have been calculated with a Debye phonon model. Fortunately, the scattered intensities involving the exchange of many phonons will be considerably less dependent on the details of the phonon spectral density than the single phonon intensities. This can be understood from Eq. (4) by noting that the nth order term in the multiphonon expansion involves an nth order convolution on the phonon spectral density, which tends to wash out all of the details. Ample experimental and theoretical evidence for this effect exists,[28,43–45,52] and this relative insensitivity to the form of the phonon spectral density is the justification for our use of the Debye model. The only important defect of the Debye model results from the fact that it overestimates the correlation at large separation distances.[28,52] In order to counteract this effect we multiply the displacement correlation function by a Gaussian influence function $\exp(-R^2/R_0^2)$, where R_0 is large compared to the lattice spacing. This eliminates numerical instabilities which can arise for small values of energy exchange and small parallel momentum exchange.

IV. EXPERIMENTAL RESULTS

A. Determination of potential parameters

Figure 2 shows two series of TOF spectra for a He atom beam with an incident energy of $E_i = 113$ meV scattered from Cu(001) along the ⟨100⟩ azimuth for surface temperatures from $T_S \simeq 120$ K up to 800 K. The measurements in Fig. 2(a) are for an angle $\Delta\theta_i = +3°$ with respect to the specular peak at 47.9°, i.e., $\theta_i = 50.9°$ and $\theta_f = 44.9°$, while the measurements in Fig. 2(b) are for $\Delta\theta_i = -3°$. Figure 3 shows a similar series of TOF spectra but for an incident energy of 82 meV. The measured intensities are compared with multiphonon calculations based on Eq. (4) for a smooth surface as discussed in Sec. III for two different sets of potential parameters. The dash–dot curves are for a set of parameters established earlier using the single phonon theory mentioned in Sec. III to fit the single phonon longitudinal resonance inelastic peak for the Cu(001) surface; $\beta = 4.7$ Å^{-1}, $Q_0 = 1.3$ Å^{-1}, and $v_R = 2000$ m/s.[22] The dashed curves are for the values of $\beta = 5.7$ Å^{-1}, $Q_0 = 2.4$ Å^{-1}, $v_R = 3000$ m/s which provided the best fit for all of the data taken in the present study. A single normalization factor was used in the comparison of calculated intensities to experimental intensities for all data taken at $E_i = 113$ meV. The calculated intensity was normalized to the experimental peak intensity for $\Delta\theta = -3°$ and $T_S = 800$ K, and the same normalization factor was used for all other angles and temperatures. In both cases the Debye temperature is taken to be $\Theta_D = 270$ K as determined previously from the Debye–Waller thermal attenuation of single phonon peak intensities.[22] Fortunately, small variations of the order of 10% or more in the value of the Debye temperature had a negligible effect on the multiphonon calculations presented here. The weighted surface phonon velocity v_R is expected to be of the order of the Raleigh wave speed, and the value used here ($v_{\text{RW}} = 3000$ m/s) is larger than the measured value of $v_{\text{RW}} = 1700$ m/s for Cu(001)⟨110⟩.[53] Table I shows a list of the potential parameters Q_c, β, and v_R together with Θ_D, which have been measured for a number of metal and insulator surfaces in both single-phonon and multiphonon studies.

The agreement between theory and experiment in Fig. 2 is quite good, especially for the best fit set of parameters, and remains almost as good for all temperatures measured except for some degradation at the very lowest temperatures. At the lowest temperatures the shape of the multiphonon TOF intensity is well represented by the theory, but the theory seems to overestimate the magnitudes of the intensities in

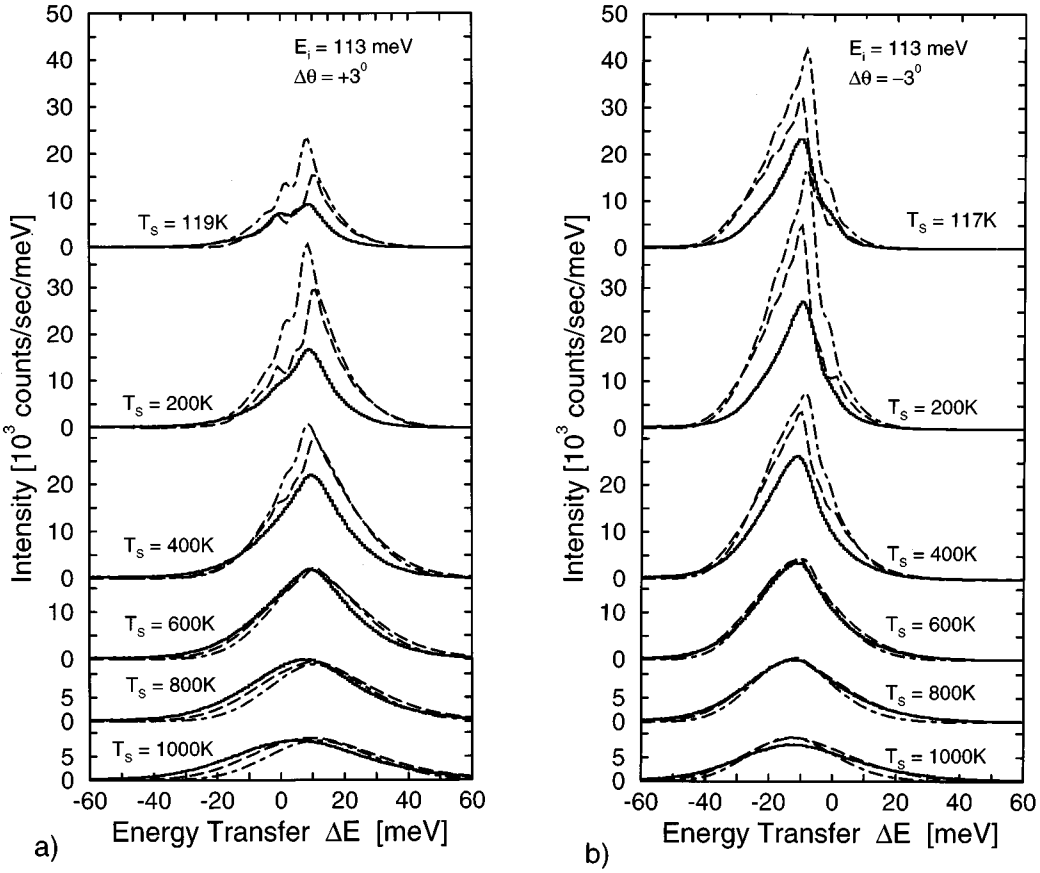

FIG. 2. A series of TOF scans, converted to an energy transfer scale, for different surface temperatures. The incident angles are $\Delta\theta_i = \pm 3°$ and the incident energy is $E_i = 113$ meV. The continuum model theory is shown by the dashed curve (---) for the set of parameters that gave the best fit for all data ($\beta = 5.7$ Å^{-1}, $Q_c = 2.4$ Å^{-1}, $v_R = 3000$ m/s, and $\Theta_D = 270$ K) and in the dash–dot curve (-·-) for the set of parameters obtained in a prior comparison with the single phonon peak intensities (Ref. 22). At low surface temperatures a large part of the difference between experiment and theory comes from the contribution of single phonon scattering which is not included in the calculation.

many cases. The calculated value of the exponent of the Debye–Waller factor for the incoherent elastic peak at $\Delta E = 0$ exchange ranges from $2W \approx 2$ for $T_S = 100$ K to $2W \approx 10$ for $T_S = 1000$ K, the latter corresponding to classical scattering. It is interesting to note that for $\Delta\theta_i = +3°$ [Fig. 2(a)] the energy transfer is positive indicating that the atom gains energy, while for $\Delta\theta_i = -3°$ [Fig. 2(b)] energy loss predominates. At $\Delta\theta_i = +3°$ and for elastic scattering ($\Delta E = 0$) the parallel momentum exchange ΔK is directed backwards (negative ΔK), and at $\Delta\theta_i = -3°$ and for zero energy exchange the ΔK is in the forward direction (positive ΔK). Both experiment and theory show slightly asymmetric peak shapes, which change from sawtoothlike at $T_S = 117$ K to nearly Gaussian at $T_S = 1000$ K.

The second series of TOF spectra shown in Fig. 3, taken along the ⟨110⟩ azimuth with a smaller incident energy of $E_i = 82$ meV, confirms this behavior. The agreement between experiment and the theory based on the same two sets of parameters as for the $E_i = 112$ meV case is again very good. As in the case of $E_i = 113$ meV, a single peak intensity normalization factor obtained from fitting experiment with theory at $\Delta\theta = -3°$ and $T_S = 800$ K was used for all calculations at this energy.

In order to check the dependence on the surface azimuth, a series of experiments were also carried out at the higher energy of 112 meV with the scattering plane along the ⟨110⟩ azimuth. The TOF spectra were nearly the same and the multiphonon calculations agree with the TOF measurements equally well as in Fig. 2.

B. Temperature dependence

After having established the optimal potential parameters for an assumed smooth surface we next investigate the surface temperature dependence of the data and its comparison with theory. Figure 4 compares the experimental and theoretical temperature dependence of the intensity at the maximum of the multiphonon peak in the TOF spectra shown in Fig. 3(a) for $E_i = 82$ meV. The dashed lines, calculated from the continuum theory of Eq. (4) for the same best fit potential parameters as Figs. 2 and 3, agree with the experimental data very well at all temperatures. At the lowest temperatures the multiphonon intensity increases with temperature thereby compensating the Debye–Waller decrease in the intensity of the elastic and single phonon inelastic quantum peaks. Thus He atoms which at lower temperatures would be scattered into the quantum peaks are diverted into the multiquantum background. However, at temperatures in

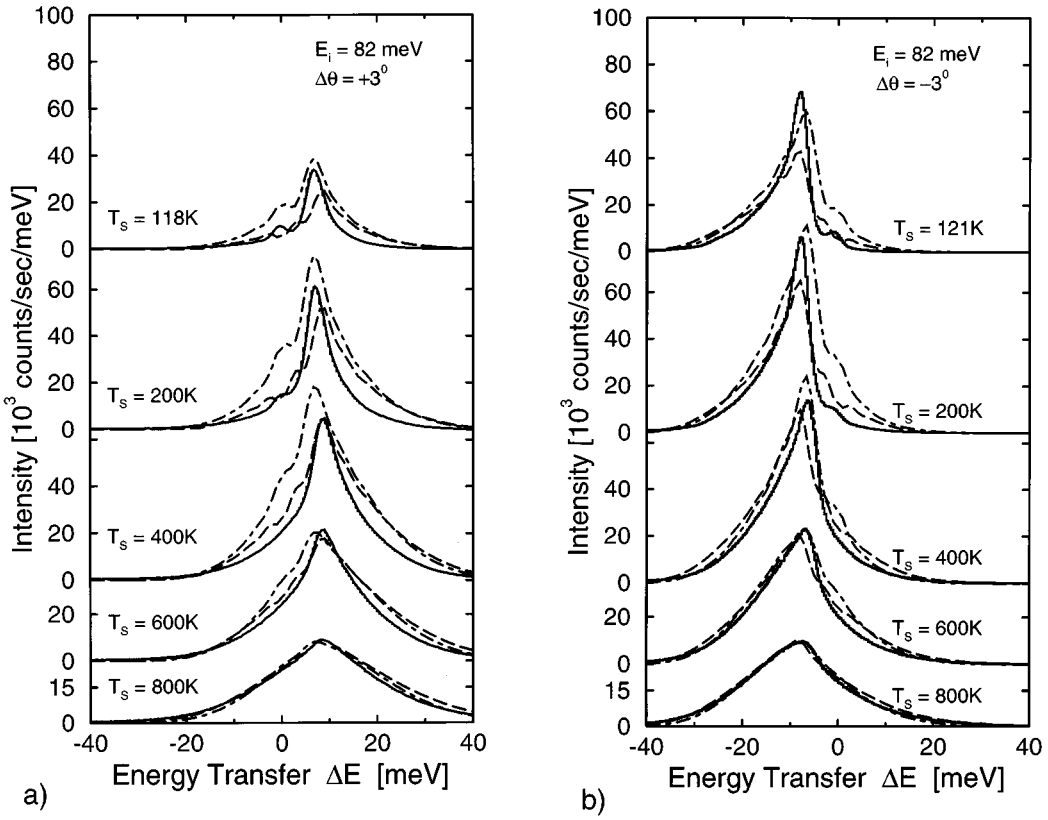

FIG. 3. A series of TOF scans converted to an energy transfer scale, as in Fig. 2, except for an incident energy of 82 meV. The calculated curves are for the same conditions as in Fig. 2.

TABLE I. Survey of all available experimentally determined potential parameters β, Q_c, v_R, and effective Debye temperatures Θ_D from both single and multiple phonon studies for several different metal and insulator surfaces. RW and LR designate values taken from studies of single-phonon Rayleigh wave and longitudinal resonance modes, respectively, and ''Multi'' designates multiphonon studies.

	Direction	Mode	β(Å^{-1})	Q_C(Å^{-1})	θ_D(K)	v_R(m/s)
Cu(001)	⟨100⟩,⟨110⟩	Multi	5.7[a]	2.4[a]	270[a]	3000[a]
Cu(001)	⟨100⟩,⟨110⟩	Multi	2.9 [52]	1.0 [52]	270 [52]	⋯
Pt(111)	⟨110⟩	Multi	1.83 [28]	0.57 [28]	231 [28]	1900 [28]
Pt(111)	⟨110⟩	Multi	2 [25]	10 [25]	250 [25]	1234 [25]
Cu(001)	⟨100⟩	RW	3.0 [22]	1.0 [22]	267 [22]	⋯
Cu(001)	⟨100⟩	LR	5.0 [22]	1.32 [22]	267 [22]	⋯
Cu(001)	⟨110⟩	RW	4.67 [22]	1.28 [22]	267 [22]	⋯
Cu(001)	⟨110⟩	LR	3.35 [22]	1.08 [22]	267 [22]	⋯
Cu(001)	⟨100⟩	RW	2.1 [54]	0.95 [54]	230 [55]	⋯
					280 [56]	⋯
Ag(001)	⟨100⟩	RW	2.77 [57]	0.87 [57]	253 [58]	⋯
Ag(001)	⟨100⟩	LR	5.30 [57]	1.20 [57]	253 [58]	⋯
Ag(001)	⟨110⟩	RW	4.85 [57]	1.15 [57]	253 [58]	⋯
Ag(001)	⟨$\underline{1}$10⟩	LR	4.12 [57]	1.06 [57]	253 [58]	⋯
Ag(111)	⟨11$\underline{2}$⟩,⟨110⟩	RW	4.0 [48]	0.74 [48]	145 [59]	⋯
Au(111)	⟨11$\underline{2}$⟩,⟨110⟩	RW	2.10 [60]	0.74 [60]	⋯	⋯
Rh(111)	⟨11$\underline{2}$⟩,⟨110⟩	RW	3.15 [61]	0.82 [61]	255 [62]	⋯
Pt(111)	⟨112⟩,⟨110⟩	RW	⋯	0.57 [63]	111 [64]	⋯
Ni(110)	⟨$\underline{1}$00⟩	RW	2.92 [65]	0.84 [65]	595 [58]	⋯
Al(111)	⟨112⟩,⟨110⟩	RW	4.0 [66]	0.92 [66]	⋯	⋯
LiF(001)	⟨100⟩	Multi	6.0 [67]	4.5 [67]	520 [67]	⋯
KCN(001)	⟨100⟩,⟨110⟩	Multi	7.5 [68]	5.5 [68]	123 [68]	⋯

[a]Present work.

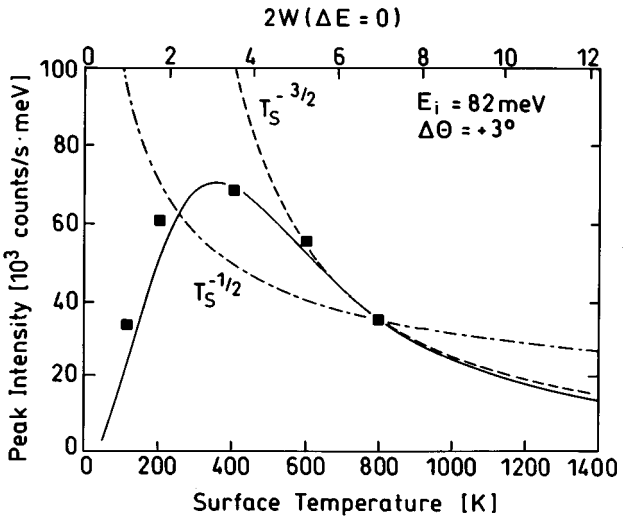

FIG. 4. Intensity at the maximum of the TOF spectra for He atoms scattered from Cu(001)⟨110⟩ as a function of surface temperature with $\Delta\theta=+3°$ and $E_i=82$ meV. The solid line (—) is from the continuum model theory with the best fit parameters ($\beta=5.7$ Å^{-1}, $Q_c=2.4$ Å^{-1}, $v_R=3000$ m/s, and $\Theta_D=270$ K). The dashed line (---) is the $T_S^{-3/2}$ envelope, and the dash–dot curve (-·-) is the $T_S^{-1/2}$ envelope. All theoretical calculations have been normalized to the experiment at 800 K. The Debye–Waller exponent at zero energy transfer is shown on the top scale.

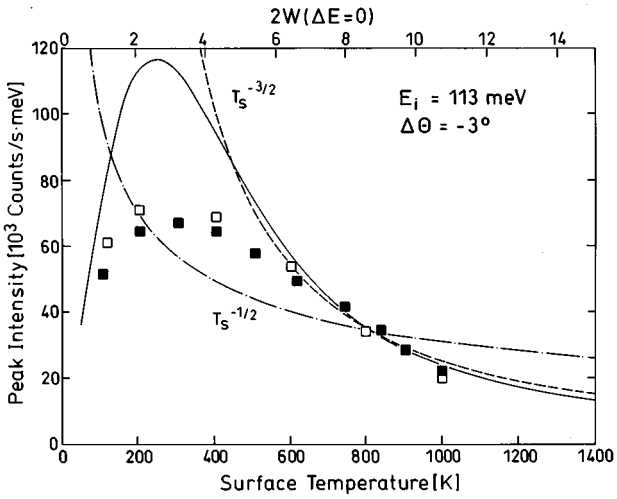

FIG. 5. Maximum multiphonon inelastic peak intensity for He scattering from Cu(001) as a function of surface temperature with $\Delta\theta=-3°$ and $E_i=113$ meV. The data are taken along the ⟨100⟩ azimuth (open data points □) and the ⟨110⟩ azimuth (filled data points ■). As in Fig. 4, the solid line (—) is from the continuum model theory with the best fit parameters, the dashed line (---) is the $T_S^{-3/2}$ envelope, and the dash–dot curve (-·-) is the $T_S^{-1/2}$ envelope. The theoretical calculations have been normalized to the experiment at 800 K. The Debye–Waller exponent calculated for the incoherent elastic peak is shown on the top scale.

the neighborhood of 500 K the maximum multiphonon intensity ceases to grow because there is no longer significant intensity in the quantum peaks to act as an effective reservoir of new multiphonon-scattered particles. At temperatures greater than 600 K the near-classical region is reached in which the multiphonon intensity continues to spread over a larger and larger energy range and consequently its maximum peak value decreases in order to conserve the total number of scattered particles.

The dashed and dash–dot curves in Fig. 4, which are both normalized to the data at 800 K display the differential reflection coefficient corresponding to the envelope functions $T_S^{-3/2}$ and $T_S^{-1/2}$, respectively, given by the continuum and discrete classical expressions of Eqs. (5) and (3). As expected the two data points at 600 and 800 K are in good agreement with the $T_S^{-3/2}$ curve for the continuum theory. Very strikingly, the $T_S^{-1/2}$ curve predicted by the discrete model does not at all agree with the data.

Figure 5 shows a comparison similar to Fig. 4 for the higher incident energy of 113 meV shown in Fig. 2(b). In this case there were many more data points and measurements were made for both the high symmetry azimuths, ⟨100⟩ and ⟨110⟩. Once again the agreement with the $T_S^{-3/2}$ envelope in the near-classical high temperature regime is quite apparent, as is the disagreement with the $T_S^{-1/2}$ envelope of the discrete model. In Fig. 5 the data point taken at $T_S=1000$ K lies a little below the calculated curve. This is most probably a manifestation of anharmonic effects, which are not included in the theory but which are known to play an increasingly important role on close-packed Cu surfaces at temperatures above 800 K.[69–72]

Anharmonicity is, however, not able to shift the experiment so as to agree with the shape of the $T_S^{-1/2}$ envelope. Evidence for this lack of significant effects of anharmonicity on the Cu(001) surface for temperatures up to at least $T_S\approx800$ K come from several sources. Earlier measurements of the Debye–Waller attenuation of the single phonon peaks of this same Cu(001) surface gave no evidence of anharmonic behavior up to the highest measured temperature of 800 K.[22] Measurements under classical conditions of the temperature dependent widths of the energy loss peaks for 200 eV Na^+ ions scattering from Cu(001) give the expected classical $T_S^{1/2}$ dependence predicted by Eqs. (3) and (5) up to $T_S\approx1000$ K with no sign of anharmonic deviation from this behavior.[73] Additional evidence for the lack of anharmonicity comes from recent molecular dynamics simulations of the Cu(001) surface[70] which completely rule out adatom–hole creation below 1000 K and show that anharmonicity becomes noticeable only well above 800 K. These theoretical results corroborate earlier experiments which also indicated that anharmonicity causes a faster than the expected Debye–Waller decrease of the elastic specular peak only at temperatures above 800 K.[72] It should be noted, however, that this observed rapid decrease of the specular peak intensity will have only little influence on the diffuse inelastic background of interest here because the actual value of the specular intensity is negligibly small at that elevated temperature (see Figs. 6 and 7).

Furthermore, we expect the effects of anharmonicity on the multiphonon intensity to be much more subtle than their well known direct effects on the single phonon intensities, or on the Debye–Waller thermal attenuation of the diffraction peak intensities. The principal effect of anharmonicity on the multiphonon intensity will be to increase the density of chan-

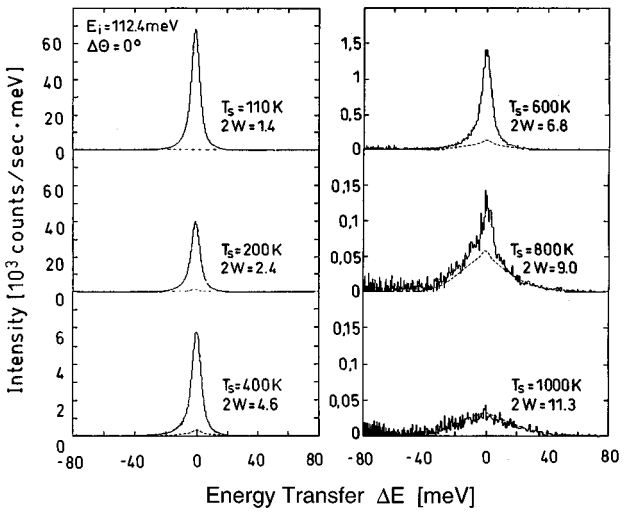

FIG. 6. A series of TOF scans at the specular position, converted to an energy transfer scale, for different surface temperatures. The incident energy is $E_i = 112.4$ meV and the measured spread at $T_S = 110$ K is the energy width of the incident beam. The continuum model theory with the best fit parameters of Figs. 2 and 3 is the dashed line. The normalization between experimental and theoretical intensities was done at $T_S = 1000$ K.

nels for inelastic scattering, which will consequently broaden the intensity distribution while simultaneously reducing its maximum peak intensity. The classical-limit differential reflection coefficients of Eqs. (3) and (5) do not depend on the actual nature of the phonon distribution because they describe the energy transfer resulting only from the initial recoil of the struck single surface atom. The increase in initial mean square displacement of the crystal due to anharmonicity would affect Eqs. (3) and (5) by augmenting T_S into a power series in T_S, making T_S effectively larger. Since both the maximum intensity and the peak width would be similarly affected, it should be observed in the peak widths as well. This, however, is not the case as will be discussed in Sec. V below.

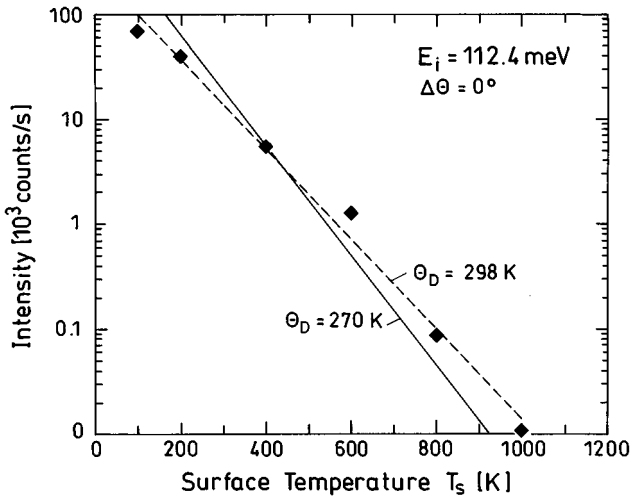

FIG. 7. A Debye–Waller plot showing the maximum intensities of Fig. 6 as a function of surface temperature. The dashed line is a linear regression to the data points and gives a Debye temperature of 298 K while the solid line is predicted for a Debye temperature of 270 K measured earlier from single phonon peaks (Ref. 22).

C. The Debye–Waller factor

Since the specular peak is a pure quantum manifestation, the transition from quantum scattering to classical scattering can be observed directly in measurements of the temperature dependence of the specular peak intensity. In Fig. 6 a series of TOF spectra as a function of the surface temperature, taken at the specular position are compared with calculations based on Eq. (4) which are shown by the dashed line curves. With increasing temperature the sharp elastic central peak decreases rapidly. Up to $T_S = 600$ K the calculated multiphonon contribution is much smaller than the measured peak intensity, but at $T_S > 800$ K the theoretical multiphonon part dominates. At $T_S = 1000$ K finally the TOF spectrum has a Gaussian-type shape without any indication of elastic scattering. Thus Fig. 6 nicely illustrates the transformation of the specular peak intensity into classical scattering intensity.

The TOF data shown in Fig. 6, after subtraction of the multiphonon background, can be used to obtain a Debye–Waller plot of specular peak intensity vs temperature and this is shown in Fig. 7. This is more difficult than the usual method of obtaining Debye–Waller plots from total intensity angular scans because of the difficulty in ascertaining perfect alignment at the maximum position of the specular diffraction peak when making the TOF measurement. The specular peak is discernible over a range of four orders of magnitude. The dashed line is a linear regression on the six data points which gives a Debye temperature of 298 K, while the solid line is the result predicted for $\Theta_D = 270$ K obtained from the more precise single phonon measurements of our earlier work.[22] This value of $\Theta_D = 270$ K was obtained from the Debye–Waller factor of both the Rayleigh mode and the longitudinal resonance mode of Cu(001) at several different incidence angles and in both the $\langle 100 \rangle$ and $\langle 110 \rangle$ surface azimuths.[22] Considering the uncertainty due to the difficulty of aligning perfectly with the maximum of the specular peak while carrying out the series of TOF measurements, the difference between the two Debye temperatures is not considered significant. Since our multiphonon calculations are insensitive to such small differences in Θ_D, as mentioned above we have consistently used the value 270 K.

D. A more critical test of the theory

The angular dependence of the scattered intensity provides a very demanding test of the quality of the theoretical modeling of the scattering process. In order to get additional data on the angular dependence and the temperature dependence of the scattered intensity with high angular resolution a series of total intensity angular distributions, shown in Fig. 8, was measured as a function of the surface temperature. At lower temperatures the angular distributions show an intense, narrow, elastic specular peak with broad wings on either side. The calculations for the multiphonon contribution, shown as dashed curves, indicate that these wings originate

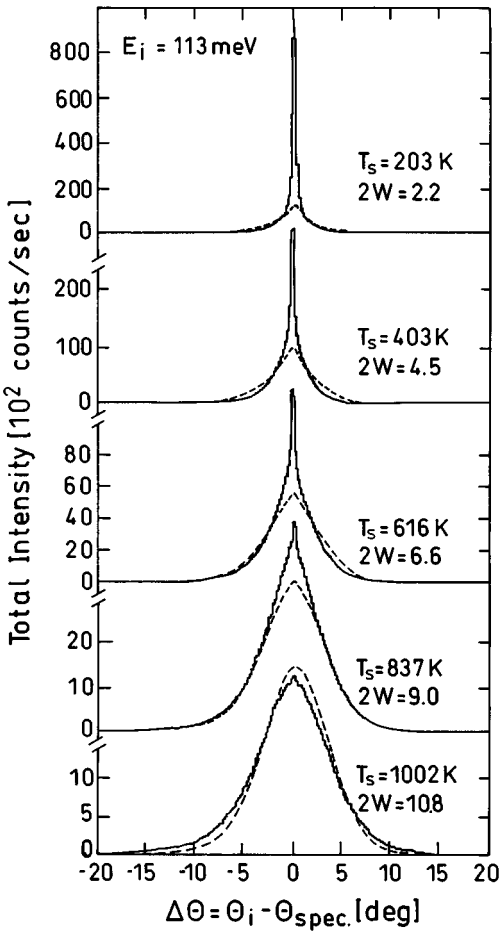

FIG. 8. A series of total intensity angular scans as a function of $\Delta\theta$ for different surface temperatures and for an incident energy of $E_i = 112.4$ meV. The continuum model theoretical calculation using the best fit parameters (dashed line) shows only the multiphonon contribution to the intensity. The normalization of calculated intensity to measured intensity is the same as for Fig. 2.

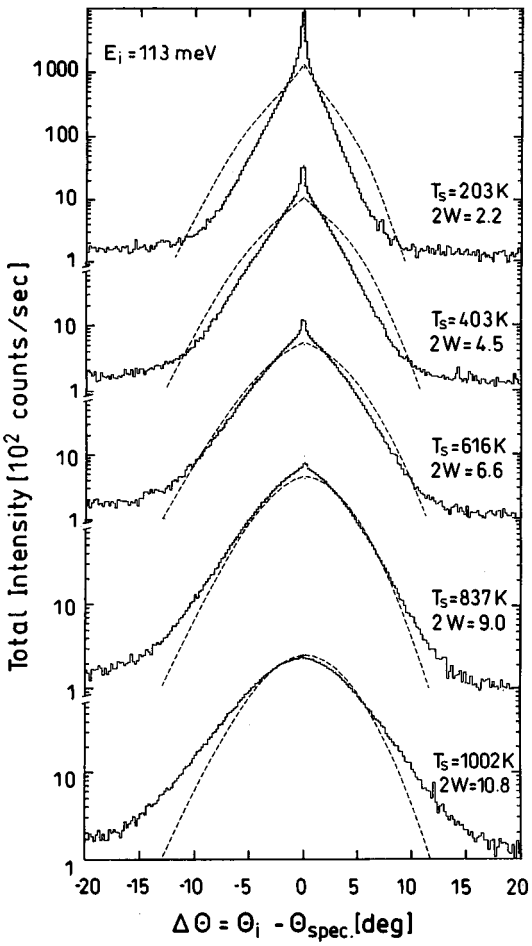

FIG. 9. Same as Fig. 8, but with a logarithmic scale.

from multiphonon inelastic scattering. As an internal test of the consistency of the experimental results, it was ascertained that the intensity at each angular position of the angular distribution was equal to the integral of the TOF measurement taken at the same angle. Thus the comparison with calculations uses the same normalization as in Fig. 2. As already shown in Fig. 6 the narrow intensity of the specular peak decreases with increasing temperature, while at the same time the intensity in the inelastic tails increases. Figure 8 reveals that this inelastic intensity is also spread over a large range of scattering angles. At $T_S = 1000$ K the specular peak has completely vanished, and the angular distribution is very close to a Gaussian shape with a full-width at half-maximum (FWHM) of 8.8°. This is in contrast to the angular distributions in the quantum regime at lower surface temperatures in which the specular peak is narrow and limited by the incident beam energy spread and geometry factors. This behavior can be seen more clearly in a logarithmic representation of the angular distributions, as presented in Fig. 9. At lower temperatures the experimental diffuse inelastic intensity falls off nearly exponentially over 3 orders of magnitude within an angular range of 10°. At intermediate temperatures the diffuse inelastic contribution broadens with increasing T_S and the fall-off on both sides changes from nearly exponential to Gaussian-type. At the highest temperature $T_S = 1000$ K all of the intensity is due to multiphonon processes and the distribution is very nearly Gaussian.

Figure 10 shows a comparison of experiment with theory for the dependence of the TOF distributions on the incident angle for a surface temperature of approximately 800 K and an incident energy $E_i = 113$ meV. The Debye–Waller exponent for elastic scattering is approximately $2W = 9$ corresponding to near classical scattering conditions. As expected from Figs. 8 and 9 the scattered intensity decays rapidly with increasing deviation $\Delta\theta$ from the specular angle at $\Delta\theta = 0$. The angular dependence of the peak position and of the peakwidth is very well described by the continuum model theory. The largest deviations occur at large $\Delta\theta$ where the small peak amplitudes are somewhat underestimated by theory.

The FWHM of the intensity vs energy transfer spectra shown in Fig. 10 are plotted as a function of temperature in Fig. 11. The FWHM is an increasing function of T_S over the entire range and theory and experiment agree well except for the very highest temperature values.

The energetic positions of the peaks in the energy trans-

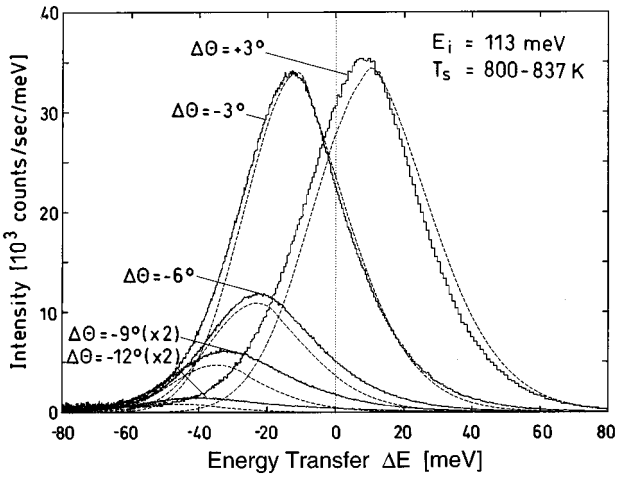

FIG. 10. A series of TOF scans, converted to an energy transfer scale, for different incident angles ranging from $\Delta\theta=+3°$ to $\Delta\theta=-12°$ and an incident energy of $E_i=112.4$ meV. The temperature is 800 K at $\Delta\theta=+3°$ and 837 K at all other angles. The continuum model theory with the best fit parameters is the dashed line.

fer spectra were observed to be nearly independent of temperature except at the highest temperatures. This is shown in Fig. 12 where the peak positions in the energy transfer spectra for the experiments carried out at $E_i=113$ meV and for all of the incident angles shown in Fig. 10 are plotted as a function of T_S. This behavior is also found to be in good agreement with the theory.

More quantitative results on the angular dependence are presented in Fig. 13, where the measured angular dependencies of the intensity at the maximum of the TOF distribution, the energy at the maximum, and the width (FWHM) for $E_i=113$ meV and $T_S=837$ K at two azimuths are compared with theoretical predictions. The intensity at the maximum of the TOF peak shows an almost Gaussian angular dependence, very similar to the total scattered intensities of Fig. 8. The lower temperature data for the ⟨100⟩ azimuth, which was measured at $T_S=800$ K, was normalized to a temperature of $T_S=837$ K by multiplying those data points by the small factor predicted by the theoretical calculations at the incident angle of $\Delta\theta=-3°$. This correction factor was very small (about 2%) for the maximum peak intensity of Fig. 13(a), and was negligible for the peak position and the FWHM of Figs. 13(b) and 13(c).

The intensity shows a Gaussian-type distribution which is peaked at $\Delta\theta=0$ in good agreement with the theory. The most probable energy transfer ΔE_{MP}, shown in Fig. 13(b) has a nearly linear dependence on the incident angle, passing through $\Delta E_{\mathrm{MP}}=0$ at $\Delta\theta=0$, with a slope of $\partial\Delta E_{\mathrm{MP}}/\partial\Delta\theta=3.3$ meV/deg, also in good agreement with the theoretical predictions. The observed peakwidth shown in Fig. 13(c) is, within the experimental errors, roughly constant at about 36 meV whereas the theory predicts a weak increase of the width with increasing incident angle. The agreement with theory is reasonably good. The downward cusp at the specular position in the calculation of Fig. 13(c) is an artifact of the calculation due to a numerical instability at this position.

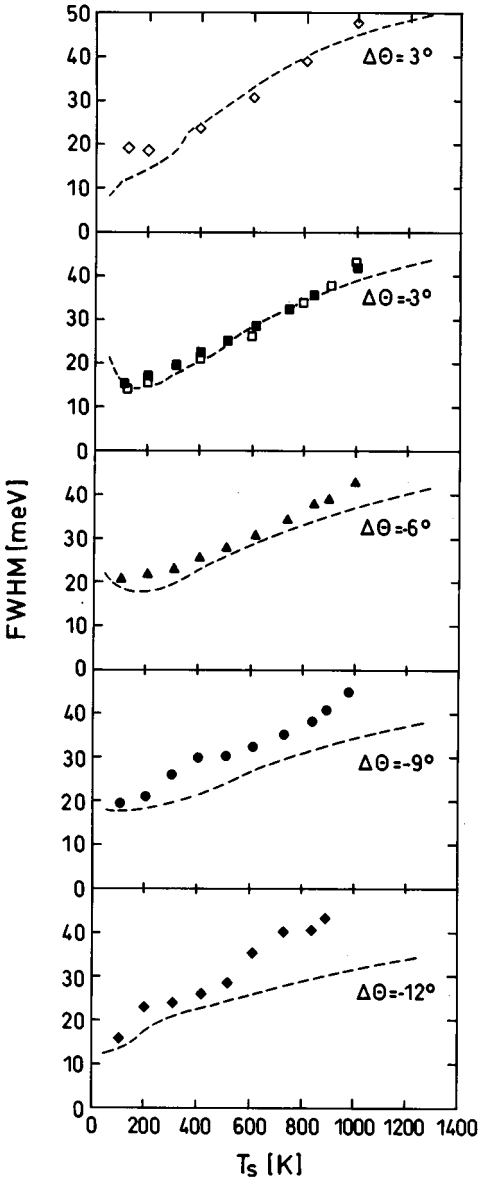

FIG. 11. The FWHM of the multiphonon intensity plotted as a function of surface temperature. The incident energy is 113 meV and data are shown for all of the incident angles of Fig. 10; the filled data points (■, ●, etc.) were measured along the ⟨110⟩ azimuth, and the open data points (□, ○, etc.) are for the ⟨100⟩ azimuth. The dashed curves are the continuum model calculation with the best fit parameters.

V. DISCUSSION

The scattering of He atoms from the Cu(001) surface has been studied for two incident beam energies of 82 meV and 113 meV for a range of surface temperatures between 100 and 1000 K. These temperatures span the complete range from the quantum mechanical regime, where the Debye–Waller exponent $2W<1$, to the classical regime in which $2W>10$. Precise TOF measurements permit a careful evaluation of the scattered intensities and energy exchange over this entire range. The energy transfer data have been compared to a quantum-mechanical theory based on interactions with the surface phonons of a smooth continuous surface. In the one-phonon limit this theory has been shown previously

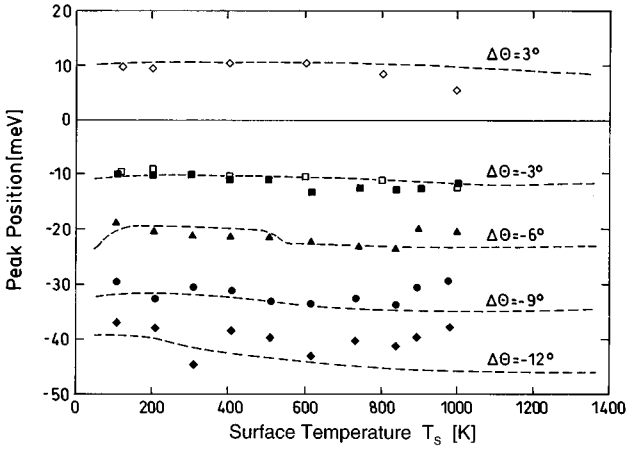

FIG. 12. The peak position of the multiphonon intensity in the energy transfer spectra plotted as a function of surface temperature. The energy, azimuthal directions, and incident angles are the same as in Fig. 11. The dashed curves are the continuum model calculation with the best fit parameters.

to describe quantitatively the energy, momentum and temperature dependencies of all single phonon peaks as well as the diffuse elastic scattering.[22]

We emphasize here that very good theoretical agreement was obtained with all of the experimental observations with only a single set of parameters for the interaction potential used to calculate the scattering form factor $|\tau_{fi}|^2$, namely with the best fit parameters $\beta=5.7$ Å^{-1}, $Q_c=2.4$ Å^{-1}, taken together with an effective surface phonon velocity $v_R=3000$ m/s. We also included for comparison in Figs. 2 and 3 calculations with a second set of parameters which were determined from earlier comparisons with the intensities of the single phonon peaks in the TOF spectra from this same Cu(001) surface; $\beta=4.7$ Å^{-1}, $Q_c=1.3$ Å^{-1}, and $v_R=2000$ m/s. As can be seen from Table I the values of the stiffness parameter β used in both calculations are relatively large compared to values determined from elastic diffraction, which are typically around $\beta=2.1$ Å^{-1}.[54] However, our value is comparable to values of β determined from measurements of single phonon scattering processes, which range as high as $\beta=5.3$ Å^{-1} for the longitudinal resonance mode of Ag(001).[57] A complete tabulation of all known β and Q_c values from inelastic measurements is given in Table I.

We note that the scattering amplitude of Eq. (6) becomes independent of β and Q_c as these parameters become large and approaches the expression for the impulsive limit for a flat hard wall[49,50]

$$\tau_{fi}=\frac{2k_{fz}k_{iz}}{m}. \tag{7}$$

For the values in the range $\beta\geqslant 4$ Å^{-1} and $Q_c\geqslant 2$ Å^{-1} used in this study, τ_{fi} is close to the limit of Eq. (7) and hence is rather insensitive to small changes in either β or Q_c. The fact that the values of β determined from single phonon inelastic measurements tend to be larger than those obtained from fitting the diffraction peaks is significant, and implies that the effective potential is stiffer for inelastic scattering.

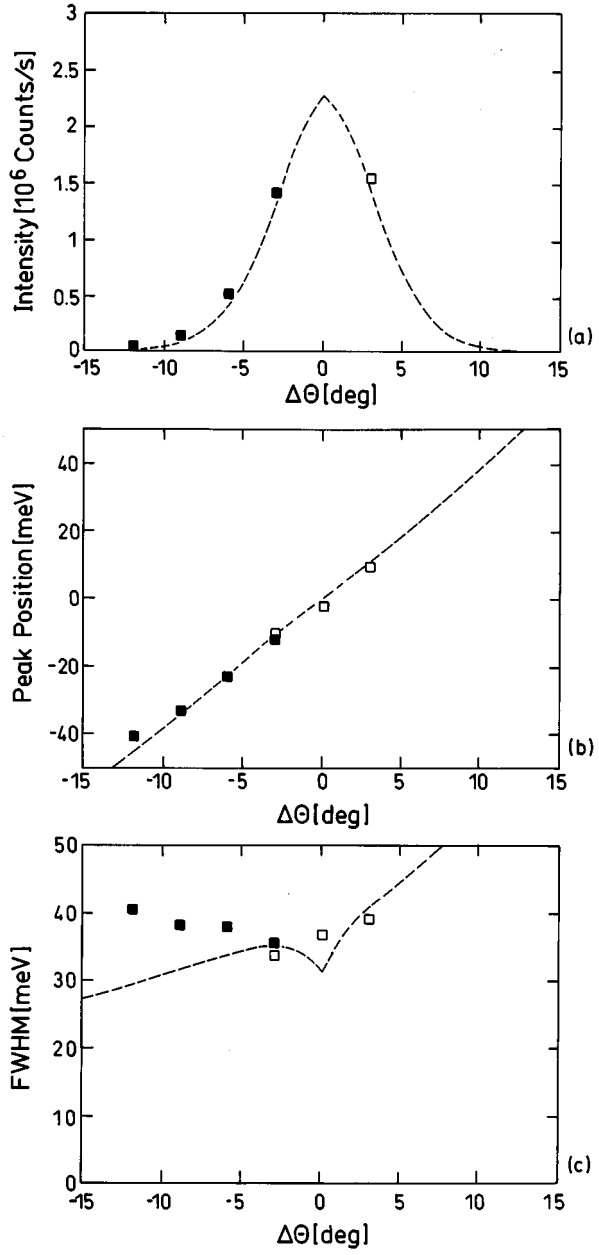

FIG. 13. Measured incident angle dependence of (a) the total intensity at the maximum of the TOF distribution, (b) the energy transfer at the maximum, and (c) the peak width (FWHM) for $E_i=113$ meV and $T_S\approx 800$ K. The data were taken along the ⟨110⟩ azimuth (filled points ■), and along the ⟨100⟩ azimuth (open points □). The dashed lines are the theoretical calculations for the continuum potential with the best fit parameters.

Our multiphonon results presented here confirm this trend and indicate that the closer the experiment approaches the limit of classical conditions, the larger the value of β will be. Further evidence of this trend is obtained from comparison with ion scattering experiments under extreme classical conditions[73] and with the high energy scattering of rare gases from liquids[74] in which good agreement between experiment and the classical limit theories of Eqs. (3) and (5) was obtained for the limit of large β and Q_c in which there is no dependence on these parameters at all.[75]

Our best fit value of $Q_c=2.4$ Å^{-1} is also larger than

typical values obtained from single phonon experiments which are usually in the range of 1 $Å^{-1}$,[48] although larger values have been reported for some single phonon measurements[22] (see Table I). A large value of Q_c implies that the scattered intensity is distributed over a wider range of wave vectors in the surface Brillouin zone. The values of β and Q_c are related by the approximate formula[48]

$$Q_c^2 = \beta / z_0 , \tag{8}$$

where z_0 is the classical turning point of the incident He projectile. The higher incident energies of this experiment would imply a somewhat smaller value for the classical turning point implying a larger value of Q_c, and similarly greater values of β would also imply larger Q_c. These arguments support the conclusion that Q_c is expected to increase with the observed increase of β as the classical multiphonon limit is approached.

The theory predicts distinct differences in the classical scattering depending upon whether the crystal is regarded as a collection of discrete scattering centers or as a continuum surface.[25] For the temperature dependence of the multiphonon envelope function, the discrete model predicts maximum intensities varying as $T_S^{-1/2}$ whereas the continuum model predicts a $T_S^{-3/2}$ dependence. The accepted model of the interaction potential between a thermal energy atom and a metal surface describes the repulsive force as being due to Pauli exchange between the atomic cloud and the tail of the metallic free electron gas extending outward from the surface.[31] Since the tail of the surface electron density appears as a continuous distribution, this would imply a continuum repulsive potential. Thus, the appropriate expressions for He scattering from a metal surface at the low energies considered here are Eqs. (4) and (5), because the potential is smooth and nearly corrugation free at the classical turning point. However, clearly this approximation will break down as the incident energy becomes larger. With increasing energy, the corrugation of the classical turning point will increase, and in the extreme high energy limit the corrugation reduces to the classical turning points surrounding the discrete crystal ionic cores. Thus with increasing energy the temperature and energy dependence of the envelope function should evolve smoothly from the $(\Delta E_0 T_S)^{-3/2}$ ''continuum'' behavior to the $(\Delta E_0 T_S)^{-1/2}$ behavior of the ''discrete'' model. In fact, there is evidence that scattering of very high energy ($\approx$200 eV) Na^+ ions from the Cu(001) surface is governed quite well by the discrete Eq. (3).[73,75] On the other hand, an intermediate case seems to be provided by the experiments of Nathanson *et al.* on the scattering of rare gases (Ne, Ar, and Xe) from liquid metals (In, Ga, and Bi). For the specific case of a 0.5 eV beam of Ar scattering from a liquid In or Ga surface over the temperature range from 300 to 500 K the temperature dependence of the inelastic maximum follows an intermediate T_S^{-1} behavior.[74,75] One can readily demonstrate theoretically that with increasing corrugation the envelope temperature dependence of the continuum model approaches that of the discrete model.[76] However, the present measurements of the multiphonon temperature dependence demonstrate convincingly that even in the classical regime He atoms are scattered from a continuum surface with no indication of scattering from a discrete lattice of individual surface atom cores.[34] This clearly shows that the projectile atoms are not exchanging vibrational energy directly with the discrete lattice of crystal atomic cores. Rather, the comparison indicates that the energy exchange at a metal surface is with the vibrations of a continuously distributed repulsive potential caused by the Pauli exchange forces with the surface electron charge density. This is in agreement with several new models for the coupling of the atoms to metal surfaces in the one-phonon limit.[29,30]

A careful examination was made for the presence of anharmonic effects in the current measurements and no evidence of anharmonicity was found up to the highest temperatures of $T_S = 1000$ K measured here. This observation has been corroborated for the Cu(001) surface by ion scattering experiments carried out entirely in the classical regime[73] and by theoretical calculations using molecular dynamics simulations.[70] It is interesting to note that, even for initial energies in the classical regime, the effects of anharmonicity appear only as a result of the thermal vibrations of the surface atoms before collision by the projectile. This can be seen in the classical limit expressions of Eqs. (3) and (5) which describe an energy exchange due to recoil of the initially vibrating surface upon collision by the incident projectile. Only after the projectile has scattered away and left the surface does the recoiling surface atom have time to transfer its energy into the rest of the crystal, presumably in the form of a cascade of phonons or electron–hole pair excitations. Thus any additional anharmonic distortion of the crystal by the incident projectile is unobservable if only the state of the scattered projectiles is detected, as is the case in these experiments. By a similar argument, in the classical limit of Eqs. (3) and (5), the scattered projectile provides no information on the creation of electron–hole pairs, again because these would be created only after the projectile has left the surface region.

This paper presents a careful study of the surface scattering of a beam of atoms in which the primary object was to investigate the transition from quantum mechanical conditions, dominated by elastic diffraction and single phonon inelastic processes, to classical conditions dominated by diffuse multiphonon energy transfer. Although measured and calculated intensities are presented here only for the case of He atoms scattering from a Cu(001) surface, the conclusions should be applicable to a large class of systems involving beams of projectiles colliding with a surface. For example, with heavier atomic projectiles such as Ne, quantum mechanical diffraction is readily observed at low temperatures and incident energies.[77–80] However, multiphonon scattering will be quite important and the transition to classical scattering will come at relatively low temperatures and incident energies, however, the methods developed here should be adequate to treat such situations. Energy exchange due to multiphonon processes is also important in molecule–surface scattering, and recent experiments on D_2 scattering from metal surfaces in the energy range $100 < E_i < 250$ meV, in addition to the expected quantum rotational transitions, ex-

hibit considerable multiphonon inelastic energy transfer which is well described by the methods used here.[81] At higher incident energies of an eV or more, comparisons to experimental data with detailed quantum mechanical calculations of the dissociative chemisorption of H_2 and D_2 on metal surfaces give evidence for substantial importance of multiphonon energy loss in the determination of the sticking coefficient.[9–12]

ACKNOWLEDGMENTS

We would like to thank G. Witte and M. Bertino for helpful discussions during the course of this work and we would like to thank S. M. Weera for help with the calculations. One of us (J.R.M.) was supported by the NSF under Grant No. DMR 9419427.

[1] M. Knudsen, Ann. Phys. **32**, 809 (1910); **34**, 593 (1911).
[2] J. P. Toennies, *Springer Series in Surface Sciences*, edited by W. Kress and F. W. de Wette (Springer, Heidelberg, 1991), Vol. 21, p. 111.
[3] G. Benedek, L. Miglio, and G. Seriani, *Springer Series in Surface Sciences*, edited by E. Hulpke (Springer, Heidelberg, 1992), Vol. 27, p. 207; R. B. Doak, *ibid*., p. 5.
[4] J. A. Barker and D. J. Auerbach, Surf. Sci. Rep. **4**, 1 (1984).
[5] G. P. Brivio and T. B. Grimley, Surf. Sci. Rep. **17**, 1 (1993).
[6] G.-P. Brivio and T. B. Grimley, Surf. Sci. Rep. **17**, 1 (1993).
[7] H. J. Kreuzer and Z. W. Gortel, *Physisorption Kinetics* (Springer, Berlin, 1896).
[8] J. Dai and J. Z. H. Zhang, J. Chem. Phys. **102**, 6280 (1995).
[9] A. Gross, J. Chem. Phys. **102**, 5045 (1995).
[10] U. Nielsen, D. Halstead, S. Holloway, and J. K. Nørskov, J. Chem. Phys. **93**, 2879 (1990).
[11] A. Gross, S. Wilke, and M. Scheffler, Phys. Rev. Lett. **75**, 2718 (1995).
[12] C. Engdahl, B. I. Lundqvist, U. Nielsen, and J. K. Nørskov, Phys. Rev. B **45**, 11 362 (1992).
[13] G. R. Darling and S. Holloway, Rep. Prog. Phys. **58**, 1595 (1995).
[14] B. Hammer, M. Scheffler, K. W. Jacobson, and J. K. Nørskov, Phys. Rev. Lett. **73**, 1400 (1994).
[15] H. F. Pfnür, C. T. Rettner, J. Lee, R. J. Maddix, and D. J. Auerbach, J. Chem. Phys. **85**, 7452 (1986).
[16] P. V. van den Hoek and E. J. Baerends, Surf. Sci. **221**, L791 (1989).
[17] J. E. Hurst, C. A. Becker, J. P. Cowin, K. C. Janda, L. Wharton, and D. J. Auerbach, J. Chem. Phys. **43**, 1175 (1979).
[18] J. E. Hurst, L. Wharton, K. C. Janda, and D. J. Auerbach, J. Chem. Phys. **83**, 1376 (1985).
[19] C. T. Rettner, E. K. Schweitzer, and C. B. Mullins, J. Chem. Phys. **90**, 3800 (1989).
[20] H.-D. Meyer and R. D. Levine, Chem. Phys. **85**, 189 (1984).
[21] J. A. Barker and C. T. Rettner, J. Chem. Phys. **97**, 5844 (1992).
[22] F. Hofmann, J. P. Toennies, and J. R. Manson, J. Chem. Phys. **101**, 10155 (1994).
[23] G. G. Bishop, W. P. Brug, G. Chern, J. Duan, S. A. Safron, J. G. Skofronick, and J. R. Manson, Phys. Rev. B **47**, 3966 (1993).
[24] A. Messiah, *Quantum Mechanics* (Academic, New York, 1969).
[25] J. R. Manson, Phys. Rev. B **43**, 6924 (1991).
[26] J. R. Manson, Comput. Phys. Commun. **80**, 145 (1994).
[27] R. Brako and D. M. Newns, Phys. Rev. Lett. **48**, 1859 (1982); Surf. Sci. **123**, 439 (1982).
[28] V. Celli, D. Himes, P. Tran, J. P. Toennies, Ch. Wöll, and G. Zhang, Phys. Rev. Lett. **66**, 3160 (1991).
[29] C. Kaden, P. Ruggerone, J. P. Toennies, G. Zhang, and G. Benedek, Phys. Rev. B **46**, 13 509 (1992).
[30] C. Kaden, P. Ruggerone, J. P. Toennies, and G. Benedek, Il Nuovo Cimento D **14**, 627 (1992).
[31] G. Vidali, G. Ihm, H.-Y. Kim, and M. W. Cole, Surf. Sci. Rep. **12**, 133 (1991).
[32] B. Salanon, G. Armand, J. Perreau, and J. Lapujoulade, Surf. Sci. **127**, 135 (1983).
[33] K. H. Rieder and N. Garcia, Phys. Rev. Lett. **49**, 43 (1982).
[34] F. Hofmann, J. P. Toennies, and J. R. Manson, Surf. Sci. **349**, L184 (1996).
[35] D. Eichenauer, U. Harten, J. P. Toennies, and V. Celli, J. Chem. Phys. **86**, 3693 (1987).
[36] H. Jónsson and J. H. Weare, Surf. Sci. **181**, 495 (1987).
[37] A. M. Lahee, W. Allison, and R. F. Willis, Surf. Sci. **147**, L630 (1984).
[38] M. Baumberger, K. H. Rieder, and W. Stocker, Surf. Sci. **167**, L203 (1986).
[39] D. M. Smilgies and J. P. Toennies, Rev. Sci. Instrum. **59**, 2185 (1988).
[40] J. R. Manson, V. Celli, and D. Himes, Phys. Rev. B **49**, 2782 (1994).
[41] V. Bortolani and A. C. Levi, Rivista del Nuovo Cimento **9**, 1 (1986).
[42] A. A. Maradudin, E. W. Montroll, and G. H. Weiss, *Theory of Lattice Dynamics in the Harmonic Approximation* (Academic, New York, 1963).
[43] G. G. Bishop, W. P. Brug, G. Chern, J. Duan, S. A. Safron, and J. G. Skofronick, Phys. Rev. B **47**, 3966 (1993).
[44] J. R. Manson, Surf. Sci. **272**, 130 (1992).
[45] J. R. Manson and J. G. Skofronick, Phys. Rev. B **47**, 12 890 (1993).
[46] A. Sjölander, Ark. Fys. **14**, 315 (1959).
[47] S. M. Weera and J. R. Manson, J. Electron Spectrosc. Relat. Phenom. **64/65**, 707 (1993).
[48] V. Celli, G. Benedek, U. Harten, J. P. Toennies, R. B. Doak, and V. Bortolani, Surf. Sci. **143**, L376 (1984).
[49] J. M. Jackson and N. F. Mott, Proc. R. Soc. London, Ser. A **137**, 703 (1932).
[50] F. O. Goodman and H. Y. Wachman, *Dynamics of Gas-Surface Scattering* (Academic, New York, 1976).
[51] V. Bortolani, A. Franchini, G. Santoro, J. P. Toennies, Ch. Wöll, and G. Zhang, Phys. Rev. B **40**, 3524 (1989); V. Bortolani, V. Celli, A. Franchini, J. Idiodi, G. Santoro, K. Kern, B. Poelsema, and G. Comsa, Surf. Sci. **208**, 1 (1989).
[52] B. Gumhalter and A. Bilić, Surf. Sci. (to be published).
[53] G. Benedek, J. Ellis, N. S. Luo, A. Reichmuth, P. Ruggerone, and J. P. Toennies, Phys. Rev. B **48**, 4917 (1993).
[54] G. Armand and J. R. Manson, Phys. Rev. B **25**, 6195 (1982).
[55] J. Lapujoulade, J. Perreau, and A. Kara, Surf. Sci. **129**, 59 (1983); G. Armand, J. Lapujoulade, and Y. Lejay, in Proceedings of the 7th International Vacuum Congress and 3rd International Conference on Solid Surfaces, Vienna 1977, edited by R. Dobrozemsky *et al.*, p. 1361 (unpublished).
[56] M. Foss, F. Besenbacher, C. Klink, and I. Stensgard, Phys. Rev. Lett. (submitted).
[57] N. Bunjes, N. S. Luo, P. Ruggerone, J. P. Toennies, and G. Witte, Phys. Rev. B **50**, 8897 (1994).
[58] J. M. Horne, C. Yerkes, and D. R. Miller, Surf. Sci. **93**, 47 (1980).
[59] G. Rovida, M. Torrini, and E. Zanizzi, Il Nuovo Cimento **4B**, 97 (1971).
[60] V. Bortolani, A. Franchini, N. Garcia, F. Nizzoli, and G. Santoro, Phys. Rev. B **28**, 7358 (1983).
[61] G. Witte, J. P. Toennies, and Ch. Wöll, Surf. Sci. **323**, 23 (1995).
[62] D. G. Castner, G. A. Somorjai, J. E. Black, D. Castiel, and R. F. Wallis, Phys. Rev. B **24**, 1616 (1981).
[63] K. Kern, Ph.D. thesis, University of Bonn, Jülich, 1985.
[64] H. B. Lyon and G. A. Somorjai, J. Chem. Phys. **44**, 3707 (1966).
[65] D. R. Haman, Phys. Rev. Lett. **46**, 1227 (1981).
[66] A. Lock, Diplom thesis, University of Göttingen, 1987; G. Benedek, Phys. Rev. B **48**, 4917 (1993).
[67] G. G. Bishop, E. S. Gillman, Jeff Baker, J. J. Hérnandez, S. A. Safron, J. G. Skofronick, S. M. Weera, and J. R. Manson, Phys. Rev. B **52**, 13 229 (1995).
[68] S. M. Weera, J. R. Manson, G. G. Bishop, E. S. Gillman, Jeff Baker, J. J. Hérnandez, S. A. Safron, and J. G. Skofronick, Phys. Rev. B **52**, 14 185 (1995).
[69] L. Yang and T. S. Rahman, Phys. Rev. Lett. **67**, 2327 (1991).
[70] T. S. Rahman and Z. J. Tian, J. Electron. Spectrosc. Relat. Phenom. **64/65**, 651 (1993).
[71] P. Zeppenfeld, K. Kern, R. David, and G. Comsa, Phys. Rev. Lett. **62**, 63 (1989).
[72] G. Armand, D. Gorse, J. Lapujoulade, and J. R. Manson, Europhys. Lett. **3**, 1113 (1987).
[73] C. A. DiRubio, D. M. Goodstein, and B. H. Cooper, Phys. Rev. Lett. **73**, 2768 (1994).
[74] W. R. Ronk, D. V. Kowalski, M. Manning, and G. M. Nathanson, J. Chem. Phys. **104**, 4842 (1996).
[75] A. Muis and J. R. Manson, Phys. Rev. B **54**, 2205 (1996).

[76] J. R. Manson (unpublished).
[77] G. Boato, P. Cantini, and L. Mattera, Surf. Sci. **55**, 141 (1976).
[78] K. H. Rieder and W. Stocker, Phys. Rev. Lett. **52**, 352 (1984); Phys. Rev. B **31**, 3392 (1985); K. H. Rieder, *ibid*. **39**, 10 708 (1989); G. Parschau, E. Kirsten, A. Bischof, and K. H. Rieder, *ibid*. **40**, 6012 (1989).
[79] E. Semerad, Surf. Sci. **211/212**, 343 (1989).
[80] B. Feuerbacher and R. F. Willis, Phys. Rev. Lett. **47**, 526 (1981).
[81] M. Bertino (unpublished).